Seeing and sensing single G-protein coupled receptors by atomic force microscopy

Tanuj Sapra[1], Patrizia Spoerri[1], Andreas Engel[1], David Alsteens[2], Daniel J. Müller[1]

[1] ETH Zürich, Department of Biosystems Science and Engineering, Mattenstrasse 26, 4058 Basel, Switzerland

[2] Louvain Institute of Biomolecular Science and Technology, Université catholique de Louvain, Croix du Sud, 4-5, bte L7.07.06., B-1348 Louvain-la-Neuve, Belgium

Corresponding author:

Daniel J. Müller
daniel.mueller@bsse.ethz.ch

Abstract

G protein-coupled receptors (GPCRs) relay extracellular information across cell membranes through a continuum of conformations that are not always captured in structures. Hence, complementary approaches are required to quantify the physical and chemical properties of the dynamic conformations linking to GPCR function. Atomic force microscopy (AFM)-based high-resolution imaging and force spectroscopy are unique methods to scrutinize GPCRs and to sense their interactions. Here, we exemplify recent AFM-based applications to directly observe the supramolecular assembly of GPCRs in native membranes, to measure the ligand-binding free-energy landscape, and how interactions modulate the structural properties of GPCRs. Common trends in GPCR function are beginning to emerge. We envision that technical developments in combining AFM with superresolution fluorescence imaging will provide insights into how cellular states modulate GPCRs and *vice versa*.

Short title

Atomic force microscopy and spectroscopy of GPCRs

Highlights

- G-protein coupled receptors regulate key physiological processes and therefore are of high interest as drug targets.
- Complementary approaches are required to obtain molecular details of the dynamic conformations of GPCRs.
- AFM-based approaches allow to directly observe and to quantify various properties of GPCRs in physiological conditions.
- FD-based AFM can image single GPCRs at high-resolution and quantify the free-energy landscape of ligand-binding.
- AFM-based force spectroscopy can structurally map the interactions of GPCRs and determine how they are altered on a complex energy landscape.

Key words

Atomic force microscopy, energy landscape, force-distance imaging, force spectroscopy, GPCR-ligand complex

Introduction

G-protein coupled receptors (GPCRs) are a versatile family of more than 800 transmembrane proteins (TMPs) [1] that sense and respond to a wide range of extracellular physical and chemical stimuli including light, neurotransmitters, odorants, hormones, and chemokines. GPCRs sense signals and transmit information across the cell membrane through a complex orchestration of conformational changes that activate and terminate intracellular signaling cascades with the help of intracellular G-proteins and arrestins, respectively [2]. Thereby GPCRs have evolved to regulate sensory responses to the environment (vision, taste, and smell) to blood pressure and heart rate, immune system activity modulation, and hemostasis. Because of their importance in defining the basic physiology of the cell and implication in neurodegenerative diseases including Alzheimer's, Parkinson's and Huntington's diseases [3], the majority of drug molecules are designed to target GPCRs [4].

The field experienced a major boost with the first X-ray structure of rhodopsin in 2000 [5]. Recent years have seen a surge in the number of GPCR structures bound to ligands, transducers, stabilized by nanobodies and mutations [6-13] highlighting the common features involved in GPCR structure, signaling and function [2, 14]. Such high-resolution structures are snapshots of discrete states of dynamic protein complexes on a complex free-energy landscape [15]. Ligand-binding, GPCR activation and inactivation are not binary 'on-off' processes but highly dynamic with conformations transitioning between energetic states on a rough energy landscape [16, 17]. To better understand the molecular details of how GPCR conformations are modulated through ligand-binding and GPCR-transducer complex (in)activation, complementary techniques need to be developed and applied.

Here we highlight atomic force microscopy (AFM)-based high-resolution (<1–2 nm) imaging and single-molecule force spectroscopy (SMFS) methods as unique complementary approaches to delve into the details of the unique and rather complex GPCR structure and function relationships. We overview recent advances in AFM methods to directly observe single native GPCRs in membranes and to quantitate their interactions with the environment at physiologically relevant conditions.

Single-molecule imaging of GPCRs in native membranes

Showing a signal-to-noise ratio superior to optical microscopes, AFM allows to directly observe single membrane proteins at sub-nanometer resolution without labeling or staining. Rhodopsin in the native membrane of discs of rod outer segments (ROS) was the first GPCR imaged by high-resolution contact mode AFM imaging in physiological buffer (**Fig. 1**). Unexpectedly, rhodopsins were observed to dimerize and to arrange in paracrystalline arrays [18]. Further AFM imaging showed that rhodopsins in human, bovine and murine ROS assemble as dimers arranged in rows forming nanodomains [19, 20]. This assembly, also confirmed by cryo-electron tomography [21], was suggested to take functional roles in facilitating signal transduction.

Multiparametric imaging of GPCRs

Conventional AFM imaging modes – contact (a scanning cantilever tip is constantly touching the protein surface) and non-contact (the tip touches the protein intermittently or not at all) modes – provide information limited to the surface topography of a protein. The recently introduced force-distance (FD) curve-based AFM (FD-AFM) can directly image single TMPs at sub-nanometer

resolution and simultaneously measure multiparametric physical and chemical properties [22, 23]. Simply, FD-AFM imaging records FD curves as the AFM cantilever tip approaches and withdraws from the sample surface (**Fig. 2a, 3a**). Each of these hundreds of thousands of FD curves quantifies the interaction forces between the tip and the sample on a high-resolution topograph. The sensitivity of the approach is sufficient to contour single membrane proteins and of their substructures including polypeptide loops [24, 25]. Operated in time-lapse mode, FD-AFM can observe single TMPs at work [26, 27] or their diffusion and supramolecular assembly [22-24] at sub-nanometer resolution [28]. Importantly, to address the complexity of TMP function, FD-AFM allows to simultaneously record the topography and to map mechanical, chemical, and biological properties.

Imaging GPCRs and quantifying their ligand-binding free-energy landscape

Conventionally, SMFS charts the ligand-binding free-energy landscape by mechanically separating single ligands bound to membrane receptors over several decades of loading rates. In FD-AFM, the ligand is tethered *via* a flexible PEG-linker to the AFM tip which allows both, the contouring of the membrane receptor with the tip and separating the ligand from the receptor while mechanically stretching the linker by withdrawing the cantilever (**Fig. 2a**). By applying a sinusoidal motion of the AFM tip, the ligand-receptor bond is ruptured at a wide range of loading rates providing the data to reconstruct the free-energy landscape. This FD-AFM approach was first applied to the human protease-activated receptor 1 (PAR1), a thrombin-activated GPCR, a key player in coagulation, hemostasis, thrombosis and inflammation [29, 30]. Thrombin cleaves the N-terminal exodomain of PAR1 and exposes the thrombin receptor-activating peptide (TRAP). TRAP remains tethered to PAR1 and acts as a ligand activating the receptor and triggering downstream signaling cascades (**Fig. 2a**). To understand the activation mechanism at molecular level, Alsteens *et al.* designed a system to mimic TRAP binding to single PAR1 receptors [29]. The SFFLRN sequence of TRAP was tethered to the cantilever tip *via* a PEG-linker to bind PAR1 during FD-AFM imaging. Approaching the cantilever to the membrane enabled binding of the SFLLRN peptide to PAR1, while retracting the cantilever gave FD curves recording the mechanically-induced unbinding process (**Fig. 2b,c**). SFFLRN-PAR1 bonds ruptured between 40–150 pN at loading rates from 4–1,100 nN/s. The distance, x_u, of the transition state barrier from the PAR1-ligand bound state was 0.6 Å. The dissociation rate, k_u, of SFFLRN at equilibrium was estimated to be ~3,621 /s and the equilibrium binding free-energy, ΔG_{bu}, was −11.22 kcal/mol corresponding to a dissociation constant K_d of ~350 nM (**Fig. 2d**), agreeing with the EC_{50} (half-maximal effective concentration) of ~800 nM from platelet aggregation assays. Changing the native SFLLRN ligand to SFLLAN decreased ΔG_{bu} to −8.61 kcal/mol and increased K_d to 30 μM, demonstrating that FD-AFM is sensitive to detect binding changes introduced by single amino acids. Another mutated peptide SALLRN decreased ΔG_{bu} to −5.73 kcal/mol and increased K_d to 3,500 μM. The results directly showed that arginine or phenylalanine in the SFLLRN sequence are crucial for high-affinity interactions with PAR1 consistent with previous functional studies [31, 32].

Quantifying ligand-binding in the presence of an antagonist

A direct application of characterizing ligand-binding to a receptor is in the presence of agonists and antagonists. Complexation of PAR1 with the antagonist vorapaxar, which attenuates platelet activation, considerably decreased the equilibrium binding free-energy, ΔG_{bu}, of SFLLRN to the receptor to –8.38 kcal/mol and the affinity of SFLLRN from ~350 nM

to ~40 μM (**Fig. 2d**) [29]. The binding-strength and -affinity of the SFLLAN peptide to PAR1 remained similar in the presence of vorapaxar suggesting that SFLLAN does not interact with the ligand-binding pocket occupied by voraxapar [7]. A possible explanation could be that vorapaxar sterically hinders the high-affinity SFLLRN-binding to PAR1 as indicated by the shorter x_u and lower ΔG_{bu} but does not block the low-affinity SFLLAN-binding site (**Fig. 2e**).

Differentiating binding of two ligands

A milestone in the development of functional FD-AFM imaging of GPCRs was to simultaneously quantify the binding of two different ligands to PAR1 (**Fig. 3**). Such differentiation is important to study how ligands compete during binding to the same receptor. Binding of an artificial ligand tris-*N*-nitrilotriacetic acid (tris-NTA) to a His_{10}-tag engineered to PAR1 and the natural ligand SFLLRN were simultaneously characterized by FD-AFM imaging (**Fig. 3**) [30]. In general, functionalizing the cantilever tip with ligands for FD-AFM of GPCRs serves many purposes: (i) single membrane receptors can be imaged at a high-resolution, (ii) ligand-binding free-energy landscapes of the native receptor can be simultaneously assayed, (iii) competitive binding of multiple ligands can be detected, and (iv) the information can be quantitatively assayed depending on the receptor's assembly and functional state, presence of chemical compounds, and membrane composition. Recently it was demonstrated that FD-AFM can also be applied to localize membrane receptors and to simultaneously characterize their free-energy landscape in living mammalian cells [33]. It is a question of time that the FD-AFM approach will be ready to study ligand-binding to GPCRs in living cells and to characterize how the binding depends on and alters the cell state.

Single-molecule force spectroscopy of GPCRs in membranes

AFM-based SMFS characterizes the mechanical and kinetic stability of the structural intermediates of GPCRs at the resolution of single α-helices [34] or a few amino acids [35]. In a nutshell, the tip of the AFM cantilever acts as a 'sticky finger' to pick up single membrane receptors from either terminal end. Pulling on the terminus by retracting the cantilever applies a mechanical force on the receptor, stepwise unfolding and extracting the receptor from the membrane [34, 36]. The FD curve recorded is a unique fingerprint of the mechanical and kinetic stability of the GPCR. The force peak pattern of these curves reacts sensitively to alterations in intra- and intermolecular interactions stabilizing a GPCR, such as of different conformations or subtle physical and chemical changes including pH, assembly, ligand-binding, mutations, and lipid membrane composition.

Bovine rhodopsin: Unfolding a GPCR paradigm

Bovine rhodopsin from ROS discs was the first GPCR characterized by SMFS [37]. It was shown that the conserved disulfide bridge (S-S) between cysteines 185 and 187 stabilizes almost all secondary structure elements within rhodopsin. Furthermore, Zn^{2+} binding at a putative extracellular site increased the mechanical stability of bovine rhodopsin and, supported by *in silico* results, suggested to favour rhodopsin dimerization [38]. These early results led to further investigating the mechanisms that mechanically (de-)stabilize GPCRs in conditions simulating (mal-)functional states.

The crystal structure of opsin shows clear differences in helical arrangements compared to dark-state rhodopsin [5, 39]. Apoprotein opsin (without 11-*cis*-retinal) shows a low constitutive activity [40] leading to retinal degeneration in Leber congenital amaurosis [41]. To understand how the

native inverse agonist, 11-*cis*-retinal, modulates the energy landscape of rhodopsin, single rhodopsins were unfolded from the ROS discs of *Rpe65 -/-* mice unable to synthesize 11-*cis*-retinal, and compared to the native dark-state rhodopsin from wild-type mice. The mechanical forces stabilizing opsin intermediates were higher than those stabilizing dark-state rhodopsin.

Unfolding a GPCR over a wide range of loading rates provides parameters, including the unfolding rate, k_u (reciprocal of lifetime), and the distance, x_u, between the native and transition states that define the free-energy landscape of a GPCR conformation. Overall, structural segments of opsin exhibited lower lifetimes (higher k_u) and lower free-energies in the range 20.6–24.5 k_BT compared to 21.5–38.0 k_BT for dark state rhodopsin. Furthermore, the structural segments of opsin were stabilized by narrower free-energy valleys (estimated by x_u) signifying the restriction of conformational states. Similarly, G90D rhodopsin, which also exhibits constitutive activity, exhibited narrower free-energy valleys, lower lifetimes and unfolding free-energy barriers compared to wild-type rhodopsin. Because both opsin and G90D rhodopsin are constitutively active, the insight gained by SMFS may signify a trend of how interactions change in native and constitutively active states. The higher energetic stability of dark state wild-type rhodopsin may lock the receptor in the inactive state which may be required for maintaining low noise and single photon sensitivity in rod photoreceptor cells.

Energy landscape of β_2-adrenergic receptor bound to agonist and antagonist

Nuanced changes in the free-energy landscape of human β_2-adrenergic receptors (β_2AR) upon agonist- and antagonist-binding were determined by SMFS. The energy landscape of β_2AR was characterized in the apo-state and in the presence of the synthetic agonists BI-167107 (BI, Boehringer Ingelheim) and THRX-144877 (THRX, Theravance), the natural agonist adrenalin, the inverse agonist carazolol, and the neutral antagonist alprenolol [42]. The distance, x_u, to the transition state from the folded state of every structural segment of apo-β_2AR ranged from 0.3 to 0.6 nm. Agonists and carazolol-binding increased the x_u of the structural core comprising helices 3 and 4, which hosts the ligand-binding sites, from 0.55 nm (unliganded β_2AR) to 0.73 nm (THRX), 0.71 nm (BI), 0.65 nm (adrenalin), and 0.79 nm (carazolol). The agonists and the inverse agonist carazolol significantly increased the kinetic stability of the core structural region. The magnitude of stability increase correlated with ligand affinity – lowest values were observed for the highest affinity ligands. ΔG_u of the unliganded β_2AR structural segments ranged from 20-23 k_BT. Ligand-binding to β_2AR core increased the ΔG_u by 7.7 k_BT (BI), 6.9 k_BT (THRX), 3.2 k_BT (adrenalin), and 7.6 k_BT (carazolol). These results suggest that the core structural segment exists on a rough energy well populated by multiple conformations suited to bind different ligands [43]. Once a ligand binds, the structural core is stabilized in a deep energy well that helps to tune β_2AR activity.

Molecular changes in PAR1 with anti-platelet agent vorapaxar

More recently, PAR1 was unfolded in the presence of different ligands to further understand the common trends in GPCR activation and inhibition [44]. PAR1 comprised structural segments (or intermediates) similar to those observed in rhodopsin and β_2AR (**Fig. 4**). Binding of vorapaxar increased the conformational variability, lifetime, free-energy, and mechanical flexibility of most structural segments (**Fig. 4e**). Furthermore, while PAR1 in the unliganded state was found to reside in a rough free-energy valley populated by many small energy wells, vorapaxar-binding smoothened the energy valley [44]. Smooth energy valleys are thought to reduce the structural

variability [45], which combined with kinetic stabilization restrict PAR1 to inactive conformations, all highlighting that vorapaxar is an effective antagonist. The changes observed in PAR1 upon antagonist-binding are consistent with the trends observed on mouse opsin, dark-state rhodopsin [46] and on human β_2AR in the presence and absence of various ligands [42]. These insights may thus highlight common mechanisms of how class A GPCRs are structurally stabilized in various states.

Role of cholesterol on GPCR stability

Single β_2AR proteins mechanically unfolded in the presence and absence of a cholesterol analog, cholesteryl hemisuccinate (CHS), showed similar structural intermediates [47]. However, CHS increased the mechanical and kinetic stability of most β_2AR structural segments except the core region which hosts the ligand-binding sites. In the presence of CHS, the intermediates were stabilized marginally and resided in energy wells 1.5–3.9 k_BT deeper with a consequent 4–50 fold increase in kinetic stability. A more stable β_2AR in a membrane with CHS suggests a role for cholesterol and lipid composition in modulating GPCR function by limiting the conformational states [47]. A decrease in stability and conformational variability in the absence of CHS may lead to faulty functioning of the receptor.

Outlook and vision

The possibility to observe individual GPCRs and to sense their interaction with ligands opens new doors in assaying how GPCRs interact with G-proteins and arrestin in signal transduction. The capability of the AFM to localize single ligand-binding events on single receptors, combined with an exceptional signal-to-noise ratio at sub-nanometer resolution, would allow to study how receptors change their interactions with ligands or other molecules and proteins in dependence to their macromolecular assembly. New developments to map ligand-binding events in living mammalian cells while simultaneously observing the cells by advanced optical microscopy techniques may soon address how GPCR states are modulated in dependence to the cell state and *vice versa*.

Mapping intermediates on the complex energy landscape of different GPCR functional states opens avenues to investigate dynamic modulation of GPCR with ligands and inhibitors. Correlating the information with functional assays may provide a more reliable basis of controlling GPCR activity with pharmacological chaperones in health and disease. This will be a focus in the future to determine the stability of GPCRs in complex with G-proteins and arrestin [48].

Acknowledgements
This work was funded by the Swiss National Science Foundation (Grant 205320_160199 and NCCR Molecular Systems Engineering) and the ETH Zürich(grant ETH-03 14-1). D.A. was supported by the Université catholique de Louvain, the European Research Council (ERC) under the European Union's Horizon 2020 research and innovation programme (grant agreement No 758224), the National Fund for Scientific Research (FNRS) and the Research Department of the Communauté française de Belgique (Concerted Research Action). D.A. is Research Associate of the FNRS.

Declaration of interest

The authors declare no conflict of interest.

References

1. Fredriksson, R. et al. (2003) The G-protein-coupled receptors in the human genome form five main families. Phylogenetic analysis, paralogon groups, and fingerprints. Mol Pharmacol 63 (6), 1256-72.
2. Hilger, D. et al. (2018) Structure and dynamics of GPCR signaling complexes. Nat Struct Mol Biol 25, 4-12.
3. Huang, Y. et al. (2017) The role of GPCRs in neurodegenerative diseases: avenues for therapeutic intervention. Curr Opin Pharmacol 32, 96-110.
4. Hauser, A.S. et al. (2017) Trends in GPCR drug discovery: new agents, targets and indications. Nat Rev Drug Discov 16, 829-842.
5. Palczewski, K. et al. (2000) Crystal structure of rhodopsin: A G protein-coupled receptor. Science 289 (5480), 739-45.
6. Choe, H.W. et al. (2011) Crystal structure of metarhodopsin II. Nature 471 (7340), 651-5.

*7. Zhang, C. et al. (2012) High-resolution crystal structure of human protease-activated receptor 1. Nature 492 (7429), 387-92.
The first X-ray crystal structure of human PAR1 stabilized with vorapaxar was reported.

8. Park, J.H. et al. (2008) Crystal structure of the ligand-free G-protein-coupled receptor opsin. Nature 454 (7201), 183-7.
9. Manglik, A. et al. (2012) Crystal structure of the micro-opioid receptor bound to a morphinan antagonist. Nature 485 (7398), 321-6.
10. Granier, S. et al. (2012) Structure of the delta-opioid receptor bound to naltrindole. Nature 485 (7398), 400-4.
11. Rasmussen, S.G. et al. (2007) Crystal structure of the human beta2 adrenergic G-protein-coupled receptor. Nature 450 (7168), 383-7.
12. Rasmussen, S.G. et al. (2011) Crystal structure of the beta2 adrenergic receptor-Gs protein complex. Nature 477 (7366), 549-55.
13. Jaakola, V.P. et al. (2008) The 2.6 angstrom crystal structure of a human A2A adenosine receptor bound to an antagonist. Science 322, 1211-1217.
14. Venkatakrishnan, A.J. et al. (2013) Molecular signatures of G-protein-coupled receptors. Nature 494, 185-194.
15. Konovalova, A. et al. (2017) Outer membrane biogenesis. Annu Rev Microbiol 71, 539-556.
16. Kobilka, B.K. and Deupi, X. (2007) Conformational complexity of G-protein-coupled receptors. Trends Pharmacol Sci 28 (8), 397-406.
17. Manglik, A. and Kobilka, B. (2014) The role of protein dynamics in GPCR function: insights from the β2AR and rhodopsin. Curr Opin Cell Biol 27, 136-143.

**18. Fotiadis, D. et al. (2003) Atomic-force microscopy: Rhodopsin dimers in native disc membranes. Nature 421 (6919), 127-8.
Based on AFM images, this paper showed for the first time that rhodopsin molecules assemble in dimers and form paracrystals in native rod outer segment membranes.

19. Whited, A.M. and Park, P.S.-H. (2015) Nanodomain organization of rhodopsin in native human and murine rod outer segment disc membranes. Biochim Biophys Acta (BBA) - Biomembranes 1848, 26-34.
20. Fotiadis, D. et al. (2004) The G protein-coupled receptor rhodopsin in the native membrane. FEBS Lett 564 (3), 281-288.
21. Gunkel, M. et al. (2015) Higher-order architecture of rhodopsin in intact photoreceptors and its implication for phototransduction kinetics. Structure 23, 628-638.

22. Dufrene, Y.F. et al. (2013) Multiparametric imaging of biological systems by force-distance curve-based AFM. Nat Methods 10 (9), 847-54.
23. Dufrêne, Y.F. et al. (2017) Imaging modes of atomic force microscopy for application in molecular and cell biology. Nat Nanotechnol 12 (4), 295-307.
24. Mulvihill, E. et al. (2018) Mechanism of membrane pore formation by human gasdermin-D. EMBO J 37 (14).
25. Pfreundschuh, M. et al. (2014) Multiparametric high-resolution imaging of native proteins by force-distance curve-based AFM. Nat Protoc 9 (5), 1113-30.
26. Muller, D.J. and Dufrene, Y.F. (2008) Atomic force microscopy as a multifunctional molecular toolbox in nanobiotechnology. Nat Nanotechnol 3 (5), 261-9.
27. Pfreundschuh, M. et al. (2013) Quantitative imaging of the electrostatic field and potential generated by a transmembrane protein pore at subnanometer resolution. Nano Lett 13 (11), 5585-5593.
28. Pfreundschuh, M. et al. (2017) Detecting ligand-Binding Events and Free Energy Landscape while Imaging Membrane Receptors at Subnanometer Resolution. Nano Lett 17, 3261-3269.

**29. Alsteens, D. et al. (2015) Imaging G protein-coupled receptors while quantifying their ligand-binding free-energy landscape. Nat Methods 12 (9), 845-51.
The first experiments demonstrating FD-AFM imaging to detect and quantify ligand binding to PAR1 receptors.

*30. Pfreundschuh, M. et al. (2015) Identifying and quantifying two ligand-binding sites while imaging native human membrane receptors by AFM. Nat Commun 6, 8857.
Two ligands on an AFM cantilever tip were used to simultaneously image PAR1 receptors, and to quantify the binding strengths of the ligands.

31. Vassallo, R.R., Jr. et al. (1992) Structure-function relationships in the activation of platelet thrombin receptors by receptor-derived peptides. J Biol Chem 267 (9), 6081-5.
32. Scarborough, R.M. et al. (1992) Tethered ligand agonist peptides. Structural requirements for thrombin receptor activation reveal mechanism of proteolytic unmasking of agonist function. J Biol Chem 267, 13146-13149.
33. Alsteens, D. et al. (2017) Nanomechanical mapping of first binding steps of a virus to animal cells. Nat Nanotechnol 12 (2), 177-183.
34. Zocher, M. et al. (2013) Single-molecule force spectroscopy of G-protein-coupled receptors. Chem Soc Rev 42 (19), 7801-15.

**35. Yu, H. et al. (2017) Hidden dynamics in the unfolding of individual bacteriorhodopsin proteins. Science 355 (6328), 945-950.
This landmark study demonstrated that AFM single-molecule force spectroscopy can unfold single α-helices of membrane proteins with amino acid resolution.

36. Bippes, C.A. and Muller, D.J. (2011) High-resolution atomic force microscopy and spectroscopy of native membrane proteins. Rep Prog Phys 74 (8), 086601.
37. Sapra, K.T. et al. (2006) Detecting molecular interactions that stabilize bovine rhodopsin. J Mol Biol 358, 255-69.
38. Park, P.S. et al. (2007) Stabilizing effect of Zn2+ in native bovine rhodopsin. J Biol Chem 282 (15), 11377-85.
39. Okada, T. et al. (2004) The retinal conformation and its environment in rhodopsin in light of a new 2.2 A crystal structure. J Mol Biol 342 (2), 571-83.
40. Melia, T.J., Jr. et al. (1997) A comparison of the efficiency of G protein activation by ligand-free and light-activated forms of rhodopsin. Biophys J 73 (6), 3182-91.

41. Woodruff, M.L. et al. (2003) Spontaneous activity of opsin apoprotein is a cause of Leber congenital amaurosis. Nat Genet 35 (2), 158-64.
42. Zocher, M. et al. (2012) Ligand-specific interactions modulate kinetic, energetic, and mechanical properties of the human beta2 adrenergic receptor. Structure 20 (8), 1391-402.
43. Deupi, X. and Kobilka, B.K. (2010) Energy landscapes as a tool to integrate GPCR structure, dynamics, and function. Physiology (Bethesda) 25 (5), 293-303.
44. Spoerri, P.M. et al. (2018) Structural properties of the human protease-activated receptor 1 changing by a strong antagonist. Structure 26, 829-838.
45. Frauenfelder, H. et al. (1991) The energy landscapes and motions of proteins. Science 254 (5038), 1598-603.
46. Kawamura, S. et al. (2013) Kinetic, energetic, and mechanical differences between dark-state rhodopsin and opsin. Structure 21 (3), 426-37.

*47. Zocher, M. et al. (2012) Cholesterol increases kinetic, energetic, and mechanical stability of the human beta2-adrenergic receptor. Proc Natl Acad Sci U S A 109 (50), E3463-72.
The paper described application of AFM single-molecule force spectroscopy in determining the effect of membrane composition on the stability of β_2-AR correlating to function.

48. Rasmussen, S.G. et al. (2011) Structure of a nanobody-stabilized active state of the beta(2) adrenoceptor. Nature 469 (7329), 175-80.

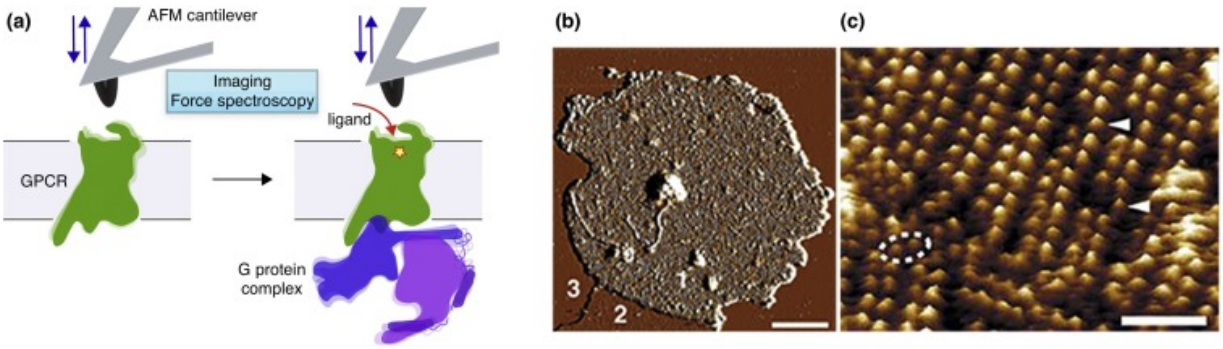

Figure 1. G protein-coupled receptors in native membranes. (a) Schematic summarizing the current and future applications of AFM imaging and force spectroscopy applied to characterize the structure and function of GPCRs in physiologically relevant conditions (buffer solution, temperature, and native or synthethic membranes). Combining the AFM imaging and force spectroscopy modes allow to directly visualize the conformation and assembly of single GPCRs and to simultaneously sense and localize individual ligand-binding events. Alternatively, the force spectroscopy mode may be used to quantify and localize intramolecular and intermolecular interactions that stabilize various functional states of the GPCR. Such functional states may be introduced by ligand-binding, mutations, lipid compositions or the presence of the G protein complex. As discussed in this review, AFM imaging and force spectroscopy of various GPCRs have been performed in the inactive and active states (with and without ligands). However, monitoring GPCR activation and interactions in presence of G protein complex remains an area for future investigations. (b) Example of imaging GPCRs in their physiologically relevant environment by AFM. Native rod outer segment (ROS) disc membrane adsorbed onto mica and imaged by contact mode AFM. Discs burst open upon exposure to osmotic shock to expose the cytoplasmic side (1). An area of empty lipid membrane (2) and the mica support (3) are also visible. Scale bar, 200 nm. (c) High-resolution AFM imaging of the membrane showing single rhodopsin molecules (white arrow heads) assembled as dimers (dashed ellipse) and arranged in rows [18]. Scale bar, 15 nm. Both images were recorded in buffer solution [18].

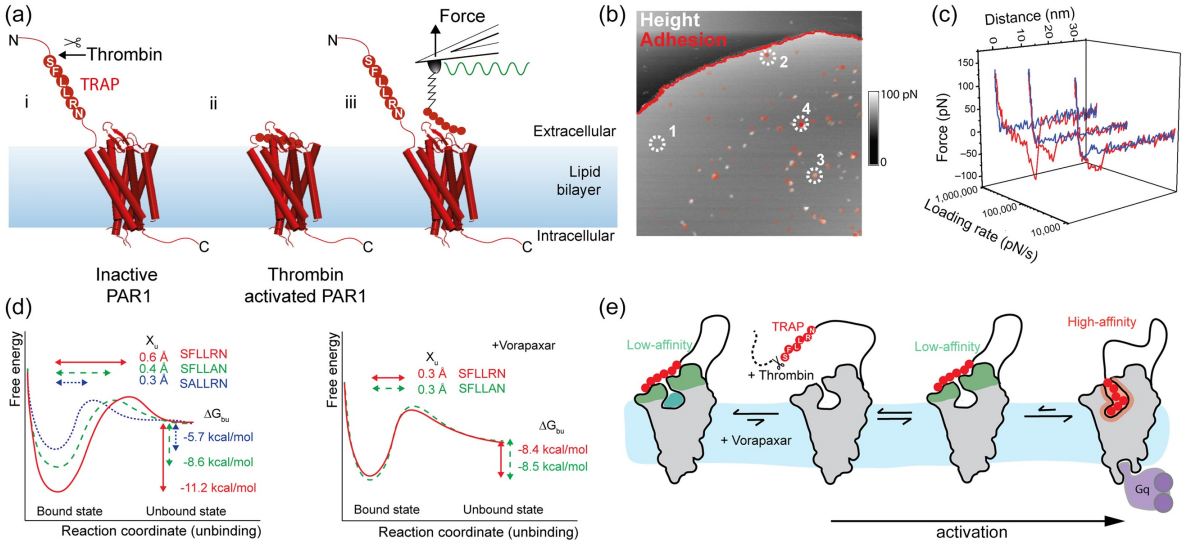

Figure 2. Ligand-binding energy landscape of PAR1 by FD-AFM imaging. (a) (i)Thrombin cleavage of the N-terminal domain of PAR1 exposes the SFLLRN sequence which acts as a tethered ligand and binds to PAR1 (ii). (iii) An AFM cantilever tip functionalized with the short peptide SFLLRN to detect interaction forces with PAR1 by FD-AFM. The cantilever is moved in a sinusoidal motion (wavy green line). (b) Collecting FD curves pixel-by-pixel in a defined grid pattern provides both, the height and the adhesion information, shown here overlaid on each other. (c) Representative FD curves recorded at different loading rates. The force peak denotes specific interactions between the peptide and PAR1 receptors. (d) Free-energy landscape showing the changes in x_u, ΔG_{bu}, because of ligand binding without (left panel) and with (right panel) the antagonist vorapaxar. (e) Model depicting the binding of the native SFLLRN ligand (red) to PAR1. For both the vorapaxar-bound and unbound states of PAR1, SFLLRN first binds with low affinity to the extracellular PAR1 surface. With vorapaxar in the binding pocket probably imposes steric hindarance to the peptide binding. However, in the absence of vorapaxar, SFLLRN can access the binding site with high-affinity, activating PAR1 and facilitating the binding of G-proteins.

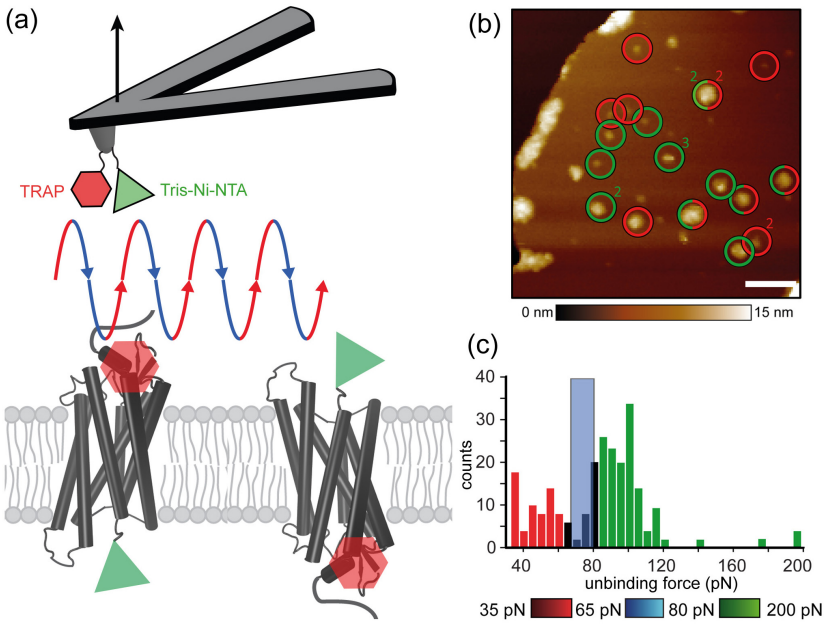

Figure 3. FD-AFM imaging of PAR1 receptors with two ligand binding. (a) The AFM cantilever tip is functionalized with two different ligands to simultaneously localize and map binding interactions on PAR1 receptors in the membrane. The cantilever is moved in a sinusoidal motion approaching (blue descending part) and retracting (red ascending part) the ligands from the PAR1 receptors. PAR1 can insert in the membrane either for TRAP to bind in the extracellar pocket (red hexagon) or tris-Ni-NTA to bind to His_{10}-tag (green triangle). (b) PAR1 in proteoliposome membrane showing sites of specific interactions between SFLLRN (TRAP)–PAR1 (red circles) on the extracellular surface and tris-NTA–His10-tag (green circles) on the intracellular surface. The numbers (2, 3) indicate that the specific interactions were detected two or three times during imaging. Scale bar, 80 nm. (c) The binding strength of both the ligands could be easily differentiated as shown by the distribution of rupture forces of SFLLRN–PAR1 (red) and of tris-NTA–His10-tag (green) bonds.

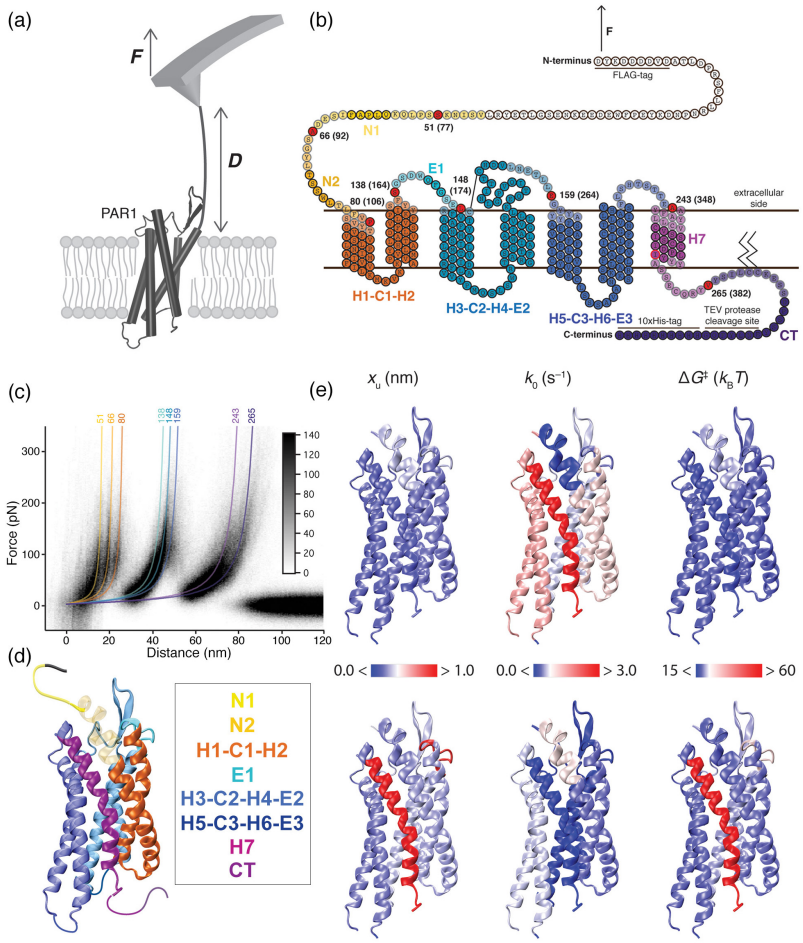

Figure 4. SMFS can differentiate the functional states of single PAR1 receptors. (a) The AFM cantilever tip is non-specifically attached to a PAR1 terminal and retracted to apply a force thereby unfolding and extracting the protein from the membrane. (b) Under an external force, the receptor unfolds in discrete steps; the structural segments that unfold individually are shown in different colors on the PAR1 secondary structure. (c) The structural segments are determined from the worm-like chain (WLC) fits (colored lines) to the force peaks of FD curves. Above the WLC fits, the contour lengths of the unfolded polypeptide are denoted in amino acids. The reproducibility of the unfolding process is determined by superimposing the FD curves. (d) Structural segments can be mapped onto the tertiary structure of PAR1 in the presence or absence of a ligand to understand the underlying molecular changes. (e) Heat maps of the energy landscape parameters of unliganded and vorapaxar-bound PAR1 mapped on the tertiary structure of PAR1 (PDB: 3VW7).